Geochemical Perspectives Letters
EAG

The journey of K-MORBs, told through geological, geochemical and geophysical data

L. Grenet[1,2,3,#*], C. Hamelin[4], D. Brunelli[5,6,7], M. Maia[1], A. Briais[1], L. Verhoest[5,1], Z. Yu[8,1,2], S.C. Singh[2]

https://doi.org/10.7185/geochemlet.2612

Abstract

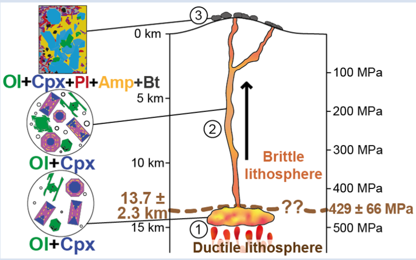

The compositional variability of mid-ocean ridge basalts (MORBs) stems from a combination of the heterogeneity of the mantle source, magma mixing, and partial crystallisation of magma in the lower crust. These variations have been mainly explored at the global and ridge scales, with only a few studies investigating them at the kilometre scale and below. Here, we focus on a series of tholeiitic to K-rich basalt samples collected during a single submarine dive near the eastern intersection between the Mid-Atlantic Ridge and the Romanche transform fault, in the equatorial Atlantic. The geochemical and petrological variations, attributed to variations in melting conditions, are extreme and consistent with the geological features. Clinopyroxene phenocrysts present in certain K-rich basalts, recorded the history of magma storage. We calculated the crystallisation pressures of clinopyroxenes and compared them to microseismicity depths recorded in the area, thus providing constraints on the lithospheric structure. This multidisciplinary work highlights the interest in exploring the composition of MORBs at high resolution to better understand the construction of the oceanic crust.

Received 25 August 2025 | Accepted 5 March 2026 | Published 13 April 2026

Introduction and Geological Context

The Mid-Atlantic Ridge (MAR) is offset by numerous transform faults (TFs) in the equatorial zone, including the large Romanche TF. The latter offsets the ridge axis by 900 km (Fig. 1a), resulting in a lithospheric age contrast of ~45 Ma and a strong cold-edge effect (Schilling *et al.*, 1994, 1995; Bonatti *et al.*, 1996, 2001; Ligi *et al.*, 2005). In addition to the local effect of the TF, the regional average temperature of the equatorial upper mantle is colder than in adjacent regions (Schilling *et al.*, 1994, 1995). A recent study based on seismic data has highlighted the presence of a thinner-than-normal crust, near the Romanche transform fault intersection with the MAR (Gregory *et al.*, 2021). Due to the combination of local and regional temperature anomalies, the degree of mantle partial melting and magma production decrease along the axis (Brunelli *et al.*, 2025), whereas lithosphere thickness increases approaching the TF (Ligi *et al.*, 2005). Basalts sampled along the ridge segments at the Eastern Romanche Ridge Transform Intersection (ERRTI) present extreme compositional variability from tholeiitic to alkaline basalts (Schilling *et al.*, 1994, 1995; Le Voyer *et al.*, 2015; Brunelli *et al.*, 2025). Brunelli *et al.* (2025) suggest that the enriched basalts are produced by reduced extents of melting of a composite mantle, where low solidus pyroxenites are dispersed in a depleted mantle. Those components may have originated from ancient dismembered sedimented oceanic crust dispersed in the mantle or from filaments of subducted oceanic plate incorporated into an ascending hot plume (Brunelli *et al.*, 2025). The processes of generation and migration of different magmas at a local scale remain poorly understood due to a lack of studies based on detailed and dense sampling.

During the SMARTIES cruise (Maia *et al.*, 2019), we explored the ERRTI volcano-tectonic setting and investigated the origin and formation of the alkaline water-rich magmas observed in the region. We focused on dive SMA1974, combining geological, geochemical, and geophysical datasets. Geochemical sampling along this dive revealed extreme variations in compositions ranging from tholeiitic to potassium-rich alkaline basalts, accompanying the variations in volcanic edifice morphology (Figs. 1, S-1). The alkaline basalts contain clinopyroxene phenocrysts, which were used in geobarometry calculations to explore the magma storage history.

1. Geo-Ocean, UMR6538 CNRS-IFREMER-UBO-UBS Institut, Universitaire Européen de la Mer IUEM, Brest, France
2. Université Paris Cité, Institut de Physique du Globe de Paris, CNRS, UMR 7154, 75005 Paris, France
3. Université de La Réunion, Laboratoire GéoSciences Réunion, CNRS, UMR 7154, 97744 Saint-Denis, France
4. Independent scholar, Sondre Skogveien 7, 5055 Bergen, Norway
5. Dipartimento di Scienze Chimiche e Geologiche, Università di Modena e Reggio Emilia, 41125 Modena, Italy
6. Woods Hole Oceanographic Institution, Woods Hole, 02543-1050 MA, USA
7. Istituto di Geologia Ambientale e Geoingegneria CNR, 00185 Roma, Italy
8. State Key Laboratory of Submarine Geoscience, Second Institute of Oceanography, Ministry of Natural Resources, Hangzhou 310012, China
Now at [2, 3]
* Corresponding author (email: lea.grenet@univ-reunion.fr)

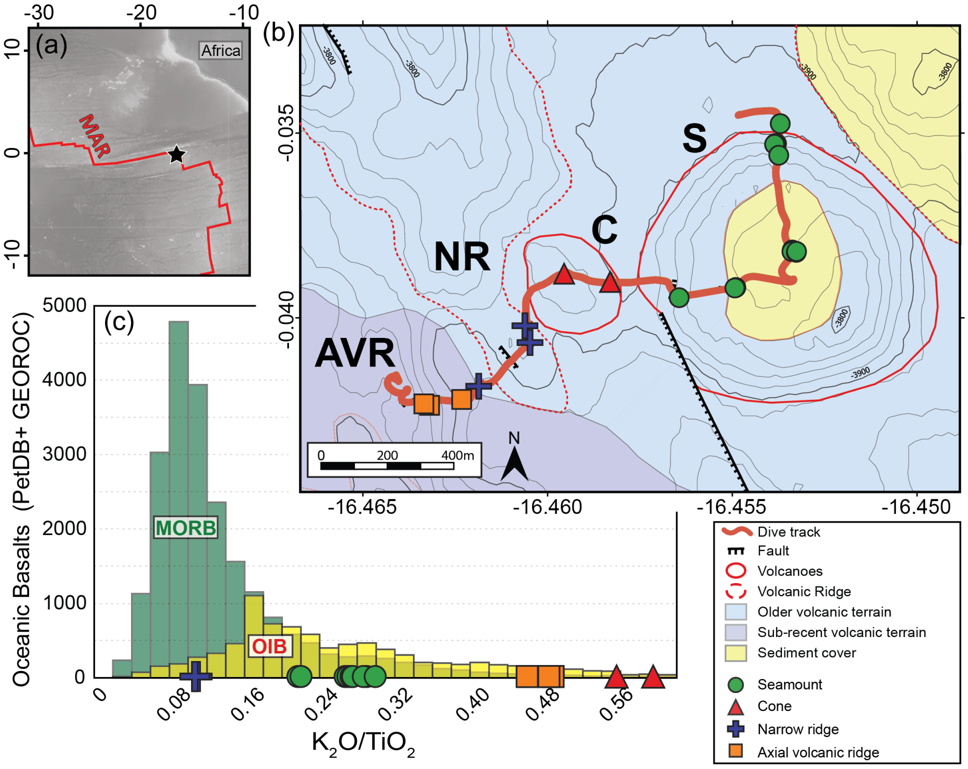

Figure 1 **(a)** Location of the ERRTI (black star). **(b)** Geological map of dive SMA1974 with the locations of the samples. S: seamount; C: cone; NR: narrow ridge; AVR: axial volcanic ridge (modified from Grenet *et al.*, 2025). **(c)** K_2O/TiO_2 ratio in samples from dive SMA1974 compared to the frequency occurrences of global mid-oceanic ridge basalts (MORB, green) and ocean island basalts (OIB, yellow) from PetDB and GEOROC datasets. Seamount and AVR data are from Brunelli *et al.* (2025).

By combining geological, geochemical, petrological, and geophysical data obtained over a small sampling area, this study provides new perspectives on our understanding of the distribution of MORB compositions through space and time and their storage conditions.

Dive SMA1974 Dataset

The ~2 km-long SMA1974 submersible dive was conducted 40 km south of the ERRTI, extending from the eastern part of the rift valley floor to the eastern flank of the axial volcanic ridge (AVR), and explored four distinct volcanic edifices: a flat-topped seamount, a small cone, a narrow volcanic ridge, and the main AVR (Figs. 1b, S-1, S-2). The cone was dated by the $^{40}Ar/^{39}Ar$ method to 135.3 ± 11.1 ka and appears to be contemporaneous with the seamount and the ridge, while the AVR seems more recent (Grenet *et al.*, 2025).

We present whole rock major and trace element analyses carried out by an inductively coupled plasma-atomic emission spectrometer and by a high-resolution inductively coupled plasma mass spectrometer, respectively. *In situ* major and trace analyses of individual minerals were performed, on polished thin sections, by electron probe microanalysis (EPMA) and laser ablation inductively coupled mass spectrometer, respectively. Geochemical maps of the samples were obtained by EPMA. The geochemical methods and thermobarometric calculations, performed on ten clinopyroxenes, are described in the Supplementary Information. Analyses of the composition of the seamount and AVR glasses were carried out by Brunelli *et al.* (2025).

Whole rock and petrological compositions. The four volcanic edifices identified during the dive have distinct petrological and geochemical characteristics (Fig. 1b-c). The narrow ridge samples are tholeiitic, while those from the cone are alkaline basalts (Figs. S-3, S-4). The samples from the seamount and the AVR have intermediate compositions. The K_2O/TiO_2 ratios of the SMA1974 dive samples extend over the entire range of global ocean basalt databases (including MORBs and OIBs, Fig. 1c).

Lavas studied here are classified as N-MORB, E-MORB, and K-MORB according to Brunelli *et al.* (2025). Samples defined as K-MORB represent a peculiar group of alkali-rich basalts reaching true alkaline, nepheline-normative compositions (Brunelli *et al.*, 2025). If oceanic basalts enriched in sodium are common in ridge settings with low degrees of partial melting, the K-MORB samples stand out because of their enrichment in potassium (Fig. S-5a). The samples from the cone and the AVR are K-MORBs (Fig. 1c), while those from the narrow ridge and the seamount are N-MORBs and E-MORBs, respectively. Trace element patterns are coherent with major elements and can be separated into distinct groups corresponding to each geological edifice (Figs. 2, S-5b and S-6).

While the tholeiitic and intermediate samples have petrological textures often observed in MORBs (aphyric to sparsely plagioclase-phyric basalts), K-MORB samples from the cone exhibit characteristics of alkali basalts. They are microlithic basalts, containing euhedral clinopyroxene phenocrysts, a low proportion of skeletal olivine phenocrysts, and hydrated, K-rich mineral phases, namely microliths of amphiboles and biotites (Figs. S-8, S-9). We also note the absence of plagioclase phenocrysts in these samples (see detailed descriptions in the Supplementary Information).

Clinopyroxene geochemistry. The clinopyroxene phenocrysts display prominent sector zoning. The hourglass sectors

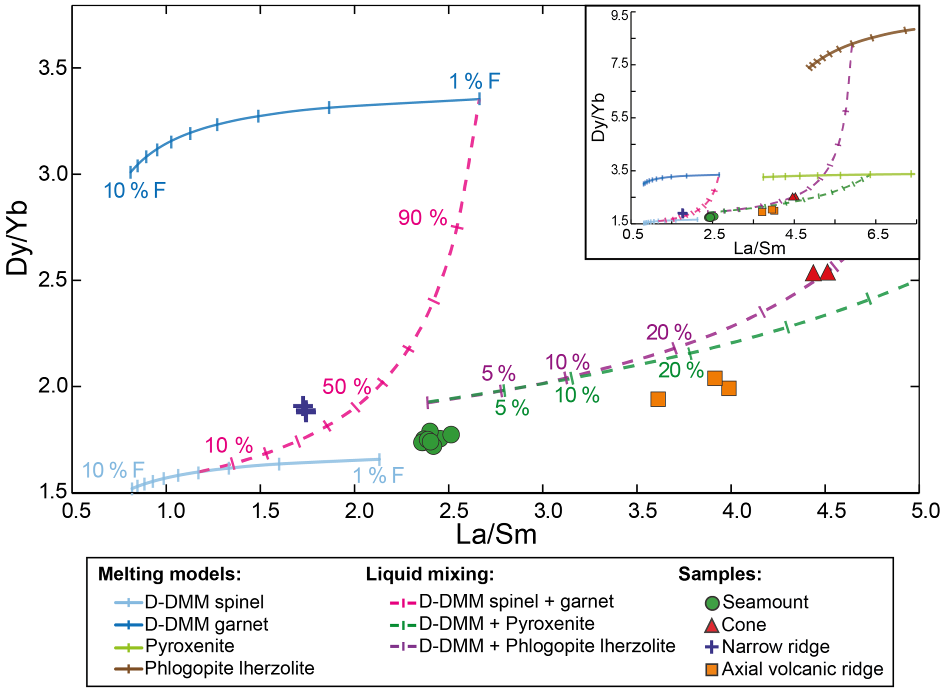

Figure 2 Plot of Dy/Yb *vs.* La/Sm for samples from dive SMA1974. Solid lines represent melting models: in blue, D-DMM in the spinel and garnet stability fields (Workman and Hart, 2005); in brown, phlogopite-bearing lherzolite in the spinel stability field (Grégoire *et al.*, 2002); and in light green, pyroxenite in the garnet stability field (G2, from Lambart, 2017). Dashed lines represent examples of liquid mixing between those melts. The parameters used are detailed in Table S-1.

have compositions enriched in Si-Mg, while the prism sectors are Al-Ti-rich (Fig. 3). Al- and Ti-rich sectors are enriched in rare earth elements and high field strength elements compared to Si-Mg-rich sectors (Table S-5).

On EPMA profiles, Cr_2O_3 peaks are observed, reaching 0.6 ± 0.006 to 1.2 ± 0.012 wt. % (Tables S-7 to S-18). These Cr peaks correlate with an increase in compatible elements (SiO_2 and MgO) and a decrease in incompatible elements (Al_2O_3 and TiO_2) compared to regular compositions (Fig. 3). Independent of the crystal sector-zoning and Cr_2O_3 peaks, concentric bands enriched in Cr_2O_3 can be observed in the geochemical maps (Fig. 3a).

Thermobarometry. The crystallisation temperatures and pressures of clinopyroxenes were iteratively estimated using Equation 33 in Putirka (2008) and Equation 1 in Neave and Putirka (2017), respectively. The equilibrium between clinopyroxenes and the whole rock was tested and considered to be reached for a $K_D = 0.03 \pm 0.08$ (Equation 35 in Putirka, 2008; Wieser *et al.*, 2023a). Component equilibria ΔDiHd, ΔEnFs, and ΔCaTs were tested using thresholds of 0.06, 0.05, and 0.03, respectively (Mollo *et al.*, 2013). The procedure was applied to the SMA1974-279 glass to evaluate the suitability of whole rock compositions for equilibrium testing. Comparable results between glass and whole rock data support the use of the latter for subsequent calculations (Table S-19). According to Zhou *et al.* (2021), in sector-zoned clinopyroxenes, the SiO_2-rich sectors are closer to real equilibrium than Al_2O_3-rich sectors. Hence, only analyses undertaken in Si-Mg-rich sectors were kept for P–T interpretations.

Melt H_2O contents were estimated using the MORB H_2O/Ce ratio from the database of Le Voyer *et al.* (2015), yielding values of 1.48 wt. % for SMA1974-278 and 1.47 wt. % for SMA1974-279.

Ten clinopyroxenes, from SMA1974-278 and SMA1974-279, satisfied all equilibrium criteria and were used for thermobarometric calculations (Figs. S-13 to S-18). Calculated temperatures range from 1112.9 to 1174.4 ± 45 °C, and pressures from 1.0 to 5.5 ± 3.8 kbar, with an average of 2.9 ± 0.9 kbar (Table S-20).

The results obtained with clinopyroxene barometers should be used with caution. Wieser *et al.* (2023a,b) highlighted the fact that these models allow only a rough distinction between crustal zones. They pointed out that considerable uncertainties arise in pressure calculations due to analytical errors related to the measurement of glass and clinopyroxene compositions and their compositional variability. To limit the effect of these errors, we tested different equilibrium criteria and used the average of at least five analysis points to obtain the crystallisation pressure of each crystal. In addition, we chose the Neave and Putirka (2017) barometer because their database is based on the analysis of >5 clinopyroxenes and is composed of Icelandic samples whose compositions are close to that of the cone (Wieser *et al.*, 2023a,b).

Discussion

Global basalt compositional variability expressed on a local scale. The range of K_2O/TiO_2 ratios along the 2-km-long SMA1974 dive is almost as large as that of global oceanic basalts (Fig. 1c). To explore which source compositions and melting conditions could account for this local geochemical variability, we calculated melting curve paths derived from non-modal batch melting involving different source compositions (Fig. 2) using Equation 15 from Shaw (2000).

The composition of the alkaline lavas cannot be accounted for by extremely low degree melting of a D-DMM source. Instead, as proposed by Verhoest (2022) and Brunelli *et al.* (2025), the generation of K-MORB requires the involvement of a pyroxenite component in the mantle source (20–40 %). Furthermore, the elevated K and H_2O contents suggest the

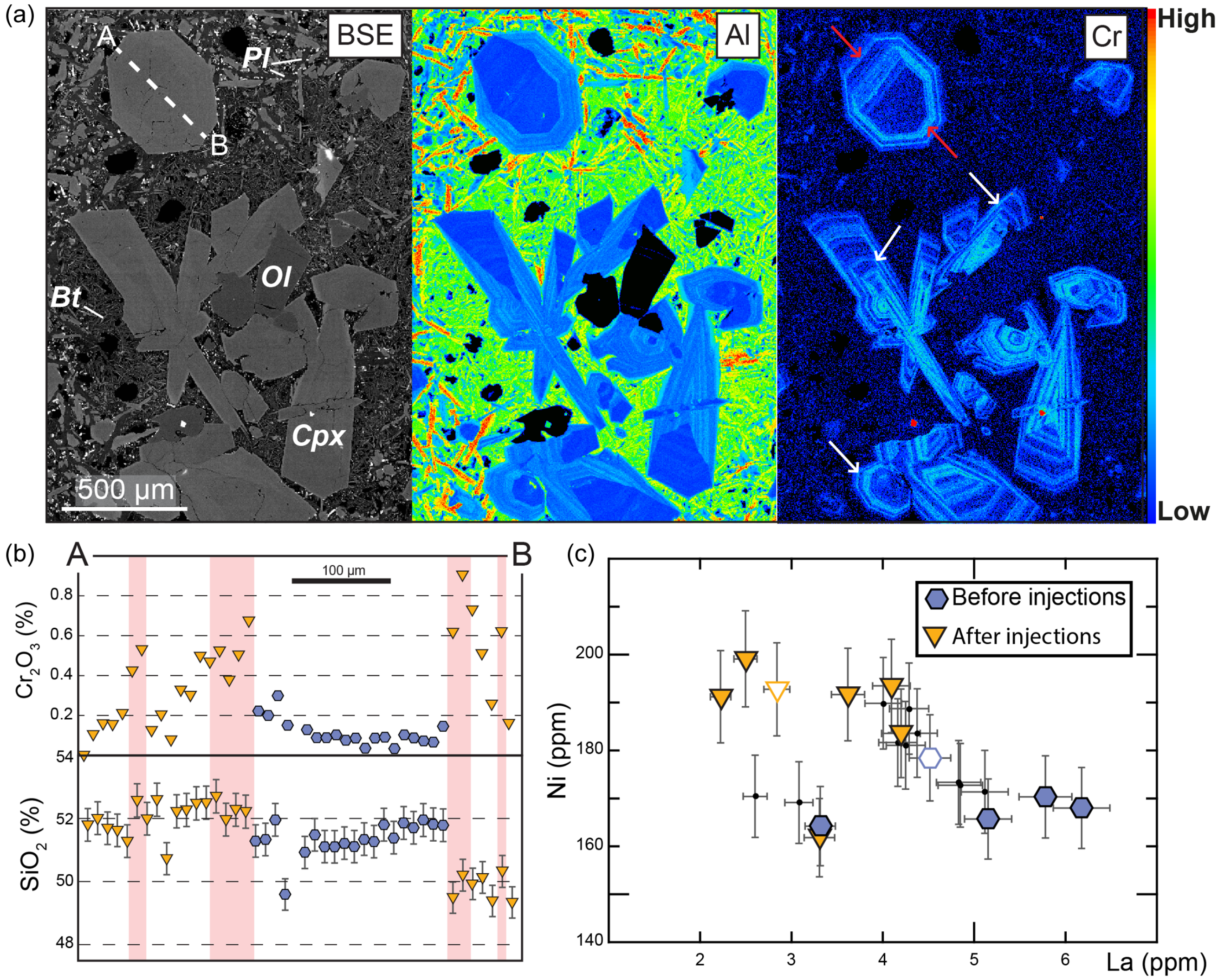

Figure 3 Major and trace element analyses of clinopyroxenes. **(a)** Left: Backscatter electron (BSE) image of a glomerophyre in SMA1974-279. The dashed line marks the trace of the profile analysis in (b). Cpx: clinopyroxene; Ol: olivine; Pl: plagioclase; Bt: biotite. Centre and right: Al and Cr element content maps, obtained by EPMA. The red arrows show the Cr_2O_3 peaks observed along the profile in (b). The white arrows present oscillatory zonation. **(b)** Cr_2O_3 and SiO_2 contents along the A–B profile. Error bars represent 1 % of the value obtained. The red bands represent the Cr_2O_3 peaks. Measurements taken with 10 µm steps. **(c)** Ni *vs.* La diagram separating analyses before and after Cr_2O_3 peaks.

presence of hydrated minerals in the K-MORB source, such as phlogopite or amphibole. Our models indicate that magma from the cone results from a mixing of melts including ~40 % liquid from melting of a phlogopite-bearing lherzolite.

These models suggest that the pronounced geochemical variability observed in SMA1974 reflects temporal changes in melting conditions of a heterogeneous mantle. Such variations occurred coevally or within a time span shorter than 135.3 ± 11.1 kyr (the estimated age of the cone).

The alkaline basalts dredged near the ERRTI also exhibit elevated volatile contents (Le Voyer *et al.*, 2015; Yu *et al.*, 2025). The high average water content (~1.5 wt. %) inferred from the H_2O/Ce ratio (Le Voyer *et al.*, 2015), support this interpretation. The elevated water content could be derived either from the mantle source itself or from the assimilation of seawater-altered crustal material. To evaluate this, we examined geochemical proxies of seawater contamination such as Cl/Nb and Cl/K in basalt glasses (Leroux *et al.*, 2006). Small contributions of seawater, linked to the source composition or by assimilation of altered crust material, would increase Cl concentration within the melt. However, all samples from dive SMA1974 have normal mantle Cl values ($Cl/Nb < 22$, Fig. S-10 and $Cl/K < 0.08$). Consistent with our melting models, these results indicate that the elevated water contents in K-MORBs reflect source heterogeneity rather than secondary contamination. Further analyses of the volatile contents of glass (H_2O, Cl and F) are required to settle this debate.

From the magmatic reservoir to the seafloor. The occurrence of clinopyroxene in basalts from the cone provides key constraints on the crystallisation and pre-eruptive evolution of these magmas. These crystals preserve the compositional record of their storage conditions during their growth. Variations in clinopyroxene Cr_2O_3 contents reveal two distinct patterns: broad Cr_2O_3-rich peaks and thin oscillatory zonation (Figs. 3 and S-11).

The high Cr_2O_3 peaks coincide with a decrease in incompatible element concentrations and enrichment in compatible elements, consistent with magma recharge by a more primitive melt (Ubide *et al.*, 2019). Nickel concentration increases immediately after Cr_2O_3-rich peaks, whereas lanthanum content decreases slightly (Fig. 3c), suggesting that the injected magma was less enriched in trace elements. The presence of pronounced sectoral zoning in clinopyroxenes, as described by MacDonald *et al.* (2024), further supports magma mixing and recharge as key processes.

The second type of Cr_2O_3 variation is thinner oscillatory zonation, not correlated with variations in compatible major elements (Fig. 3a). Crystallisation experiments show that active convection supplies fresh Cr-cations to the melt–crystal interface, which are incorporated into low-amplitude concentric bonds (Di Fiore *et al.*, 2021). This observation suggests that those clinopyroxenes crystallised in a dynamic convective reservoir (Petrone *et al.*, 2022).

Estimation of the lithosphere brittle–ductile boundary depth: agreement between geochemistry and geophysics. We took advantage of the presence of clinopyroxenes in the cone samples to estimate their crystallisation pressure and compare our results to the depths estimated by microseismicity. Given the limited number of clinopyroxenes analysed, the use of whole rock composition, the limits of the barometers, and the fact that the seismic data was only collected over a short period, further work is needed to confirm these depths on a regional scale.

Microseismicity recorded by ocean bottom seismometers (OBS) in this segment (Yu *et al.*, 2025), shows some events with focal depths between 9.1 ± 3.3 km and 19.3 ± 4.3 km below the seafloor (Figs. 4 and S-2). This is deeper than would be expected (<8 km) under regular slow-spreading ridges (Grevemeyer *et al.*, 2019). Based on the basalt chemical composition in samples from this segment, Yu *et al.* (2025) predicted a high concentration of volatiles in primary melts in this region and proposed CO_2 exsolution in deep melts as a potential origin of the deep microseismicity.

Since we do not know the exact proportion of volcanic crust and lithospheric mantle in our region, we calculated the crystallisation depths using densities of 2.8 g/cm^3 (basalt-dominated lithosphere) and 3.3 g/cm^3 (ultramafic lithosphere). We acknowledge that a realistic value should be somewhere in between. The calculated crystallisation depths range from 6.2 ± 2.6 km to 13.8 ± 2.3 km below the seafloor (Fig. 4, Table S-20). The variability in crystallisation depths could be due to the magma stagnating at different levels, possibly in small pockets, on its way to the surface. These depths are consistent with the current depth of microseismicity located between four and six kilometres west to southwest of the cone (Figs. 4 and S-2).

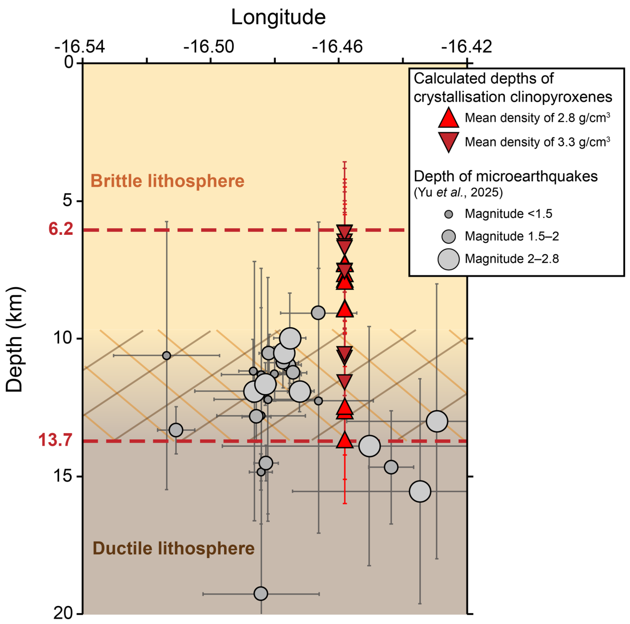

Figure 4 Calculated crystallisation depths of clinopyroxenes and microearthquake depths (Yu *et al.*, 2025), plotted according to longitude. The composition of the ten clinopyroxenes was measured at different points on each of the minerals. The average depth and the 1σ standard deviation were calculated for each clinopyroxenes.

Beneath mid-ocean ridges, liquids can coalesce into small, temporary pockets under permeable barriers such as the lithosphere brittle–ductile boundary (BDB). In our study area, the depth of these potential pockets corresponds to the greatest microseismic activity and crystallisation depths (6–15 km). Assuming the base of the oceanic brittle lithosphere is at the 750 °C isotherm (Phipps Morgan and Chen, 1993), the local thermal model from Ligi *et al.* (2005) predicts a BDB depth of ~10 km. The depths of the pockets, based on both thermobarometry and microseismicity, appear consistent with the estimated depth range of the BDB. These estimated magmatic reservoir depths are greater than those obtained in other part of the MAR (3–4 km; Wanless *et al.*, 2015), which is consistent with the strong cold-edge effect expected close to the Romanche TF.

While microseismicity and crystallisation depths are comparable, these two datasets are snapshots taken at two different times. Clinopyroxenes used for geobarometric calculations were sampled from a lava flow dated at 135.3 ± 11.1 ka. Meanwhile, the microseismicity was recorded by OBSs in 2019. We may hypothesise that the depth of the magma accumulation and differentiation, remained stable over this stretch of time.

Conclusions

We explored in detail a section of the slow-spreading MAR at its eastern intersection with the Romanche TF, combining geological, geochemical, petrological, and geophysical data. The basalts from the studied submersible dive exhibit extreme geochemical variability, almost as large as that of global oceanic basalts. Those variations are coherent with the morphology of the individual volcanic edifices observed in this area. These compositions and their distribution can be related to different eruptive events characterised by specific mantle compositions and melting conditions. The clinopyroxenes present in some K-MORBs recorded mixing events during the magma storage. Furthermore, the crystallisation depths of these clinopyroxenes are consistent with geophysics, suggesting that the depth of the BDB is 10–15 km below the seafloor and has remained stable over 135 kyr.

Acknowledgements

We are grateful to the officers, crew, and scientific party for their hard work during the 2019 SMARTIES cruise onboard the R/V *Pourquoi Pas?*. The ship time for the SMARTIES cruise (Maia *et al.*, 2019; https://doi.org/10.17600/18001107) was granted by the TGIR French Oceanographic Fleet. This work was financially supported by CNRS-INSU Tellus "Campagnes à la mer" and "SYSTER" programs, Région Bretagne and by the ISblue project, Interdisciplinary graduate school for the blue planet (ANR-17-EURE-0015) and co-funded by a grant from the French government under the program "Investissements d'Avenir". We thank the editor, Helen Williams, and Hugh O'Neill, Joshua Shea, and an anonymous reviewer for their constructive comments and suggestions, which greatly improved our manuscript.

Editor: Helen Williams

Additional Information

Supplementary Information accompanies this letter at https://www.geochemicalperspectivesletters.org/article2612.

Cite this letter as: Grenet, L., Hamelin, C., Brunelli, D., Maia, M., Briais, A., Verhoest, L., Yu, Z., Singh, S.C. (2026) The journey of K-MORBs, told through geological, geochemical and geophysical data. *Geochem. Persp. Let.* 39, 48–53. https://doi.org/10.7185/geochemlet.2612

References

Bonatti, E., Ligi, M., Carrara, G., Gasperini, L., Turko, N., Perfiliev, S., Peyve, A., Sciuto, P.F. (1996) Diffuse impact of the Mid-Atlantic Ridge with the Romanche transform: an ultracold ridge-transform intersection. *Journal of Geophysical Research: Solid Earth* 101, 8043–8054. https://doi.org/10.1029/95JB02249

Bonatti, E., Brunelli, D., Fabretti, P., Ligi, M., Asunta Portaro, R., Seyler, M. (2001) Steady-state creation of crust-free lithosphere at cold spots in mid-ocean ridges. *Geology* 29, 979. https://doi.org/10.1130/0091-7613(2001)029<0979:SSCOCF>2.0.CO;2

Brunelli, D., Verhoest, L., Ligi, M., Hemond, C., Maia, M., Soltanmohammadi, A., Lugli, F., Nonnotte, P., Cipriani, A. (2025) Large melt diversity at a mid-ocean ridge thermal low. *Science Advances* 11. https://doi.org/10.1126/sciadv.adv4654

Di Fiore, F., Mollo, S., Vona, A., MacDonald, A., Ubide, T., Nazzari, M., Romano, C., Scarlato, P. (2021) Kinetic partitioning of major and trace cations between clinopyroxene and phonotephritic melt under convective stirring conditions: New insights into clinopyroxene sector zoning and concentric zoning. *Chemical Geology* 584, 120531. https://doi.org/10.1016/j.chemgeo.2021.120531

Grégoire, M., Bell, D., Le Roex, A. (2002) Trace element geochemistry of phlogopite-rich mafic mantle xenoliths: their classification and their relationship to phlogopite-bearing peridotites and kimberlites revisited. *Contributions to Mineralogy and Petrology* 142, 603–625. https://doi.org/10.1007/s00410-001-0315-8

Gregory, E.P.M., Singh, S.C., Marjanović, M., Wang, Z. (2021) Serpentinized peridotite versus thick mafic crust at the Romanche oceanic transform fault. *Geology* 49, 1132–1136. https://doi.org/10.1130/G49097.1

Grenet, L., Maia, M., Hamelin, C., Briais, A., Guillou, H., Scao, V., Brunelli, D. (2025) A Deep Dive Into a Ridge-Transform Fault Intersection: Volcano-Tectonic Relationships in an Enhanced Cold-Edge Effect at the Romanche Fracture Zone. *Journal of Geophysical Research: Solid Earth* 130. https://doi.org/10.1029/2024JB030688

Grevemeyer, I., Hayman, N.W., Lange, D., Peirce, C., Papenberg, C., Van Avendonk, H.J.A., Schmid, F., De La Peña, L.G., Dannowski, A. (2019) Constraining the maximum depth of brittle deformation at slow- and ultra-slow-spreading ridges using microseismicity. *Geology* 47, 1069–1073. https://doi.org/10.1130/G46577.1

Lambart, S. (2017) No direct contribution of recycled crust in Icelandic basalts. *Geochemical Perspectives Letters* 4, 7–12. https://doi.org/10.7185/geochemlet.1728

Le Voyer, M., Cottrell, E., Kelley, K.A., Brounce, M., Hauri, E.H. (2015) The effect of primary versus secondary processes on the volatile content of MORB glasses: An example from the equatorial Mid-Atlantic Ridge (5°N–3°S). *Journal of Geophysical Research: Solid Earth* 120, 125–144. https://doi.org/10.1002/2014JB011160

Leroux, P., Shirey, S., Hauri, E., Perfit, M., Bender, J. (2006) The effects of variable sources, processes and contaminants on the composition of northern EPR MORB (8–10°N and 12–14°N): Evidence from volatiles (H2O, CO2, S) and halogens (F, Cl). *Earth and Planetary Science Letters* 251, 209–231. https://doi.org/10.1016/j.epsl.2006.09.012

Ligi, M., Bonatti, E., Cipriani, A., Ottolini, L. (2005) Water-rich basalts at mid-ocean-ridge cold spots. *Nature* 434, 66–69. https://doi.org/10.1038/nature03264

MacDonald, A., Ubide, T., Mollo, S. (2024) Degree of sector zoning in clinopyroxene records dynamic magma recharge and ascent. *Geochimica et Cosmochimica Acta* 378, 245–258. https://doi.org/10.1016/j.gca.2024.06.025

Maia, M., Brunelli, D., Ligi, M. (2019) SMARTIES cruise, RV Pourquoi pas ? https://doi.org/10.17600/18001107

Mollo, S., Putirka, K., Misiti, V., Soligo, M., Scarlato, P. (2013) A new test for equilibrium based on clinopyroxene–melt pairs: Clues on the solidification temperatures of Etnean alkaline melts at post-eruptive conditions. *Chemical Geology* 352, 92–100. https://doi.org/10.1016/j.chemgeo.2013.05.026

Neave, D.A., Putirka, K.D. (2017) A new clinopyroxene-liquid barometer, and implications for magma storage pressures under Icelandic rift zones. *American Mineralogist* 102, 777–794. https://doi.org/10.2138/am-2017-5968

Petrone, C.M., Mollo, S., Gertisser, R., Buret, Y., Scarlato, P., Del Bello, E., Andronico, D., Ellis, B., Pontesilli, A., De Astis, G., Giacomoni, P.P., Coltorti, M., Reagan, M. (2022) Magma recharge and mush rejuvenation drive paroxysmal activity at Stromboli volcano. *Nature Communications* 13, 7717. https://doi.org/10.1038/s41467-022-35405-z

Phipps Morgan, J., Chen, Y.J. (1993) Dependence of ridge-axis morphology on magma supply and spreading rate. *Nature* 364, 706–708. https://doi.org/10.1038/364706a0

Putirka, K.D. (2008) Thermometers and Barometers for Volcanic Systems. *Reviews in Mineralogy and Geochemistry* 69, 61–120. https://doi.org/10.2138/rmg.2008.69.3

Schilling, J.-G., Hanan, B.B., McCully, B., Kingsley, R.H., Fontignie, D. (1994) Influence of the Sierra Leone mantle plume on the equatorial Mid-Atlantic Ridge: A Nd-Sr-Pb isotopic study. *Journal of Geophysical Research: Solid Earth* 99, 12005–12028. https://doi.org/10.1029/94JB00337

Schilling, J.-G., Ruppel, C., Davis, A.N., McCully, B., Tighe, S.A., Kingsley, R.H., Lin, J. (1995) Thermal structure of the mantle beneath the equatorial Mid-Atlantic Ridge: Inferences from the spatial variation of dredged basalt glass compositions. *Journal of Geophysical Research* 100, 10057–10076. https://doi.org/10.1029/95JB00668

Shaw, D.M. (2000) CONTINUOUS (DYNAMIC) MELTING THEORY REVISITED. *The Canadian Mineralogist* 38, 1041–1063. https://doi.org/10.2113/gscanmin.38.5.1041

Ubide, T., Mollo, S., Zhao, J., Nazzari, M., Scarlato, P. (2019) Sector-zoned clinopyroxene as a recorder of magma history, eruption triggers, and ascent rates. *Geochimica et Cosmochimica Acta* 251, 265–283. https://doi.org/10.1016/j.gca.2019.02.021

Verhoest, L. (2022) Melting a heterogeneous Earth's mantle under an extreme thermal gradient. Doctoral dissertation, Université de Bretagne occidentale-Brest; Università degli studi di Modena e Reggio Emilia. https://theses.hal.science/tel-05351687

Wanless, V.D., Shaw, A.M., Behn, M.D., Soule, S.A., Escartín, J., Hamelin, C. (2015) Magmatic plumbing at Lucky Strike volcano based on olivine-hosted melt inclusion compositions. *Geochemistry, Geophysics, Geosystems* 16, 126–147. https://doi.org/10.1002/2014GC005517

Wieser, P.E., Kent, A.J.R., Till, C.B. (2023a) Barometers Behaving Badly II: a Critical Evaluation of Cpx-Only and Cpx-Liq Thermobarometry in Variably-Hydrous Arc Magmas. *Journal of Petrology* 64, egad050. https://doi.org/10.1093/petrology/egad050

Wieser, P.E., Kent, A.J.R., Till, C.B., Donovan, J., Neave, D.A., Blatter, D.L., Krawczynski, M.J. (2023b) Barometers Behaving Badly I: Assessing the Influence of Analytical and Experimental Uncertainty on Clinopyroxene Thermobarometry Calculations at Crustal Conditions. *Journal of Petrology* 64, egac126. https://doi.org/10.31223/X5JT0N

Workman, R.K., Hart, S.R. (2005) Major and trace element composition of the depleted MORB mantle (DMM). *Earth and Planetary Science Letters* 231, 53–72. https://doi.org/10.1016/j.epsl.2004.12.005

Yu, Z., Singh, S.C., Hamelin, C., Grenet, L., Maia, M., Briais, A., Petracchini, L., Brunelli, D. (2025) Deep mantle earthquakes linked to CO_2 degassing at the mid-Atlantic ridge. *Nature Communications* 16, 563. https://doi.org/10.1038/s41467-024-55792-9

Zhou, J.-S., Wang, Q., Xing, C.-M., Ma, L., Hao, L.-L., Li, Q.-W., Wang, Z.-L., Huang, T.-Y. (2021) Crystal growth of clinopyroxene in mafic alkaline magmas. *Earth and Planetary Science Letters* 568, 117005. https://doi.org/10.1016/j.epsl.2021.117005